Cell Size as a Primary Determinant in Targeted Nanoparticle Uptake

Douglas Howard[1], *Tyron Turnbull*[1], *David J. Paterson*[2], *Benjamin Thierry*[1], *Ivan Kempson*[1*]

[1]Future Industries Institute, University of South Australia, Mawson Lakes, SA 5095, Australia

[2]Australian Synchrotron, ANSTO, 800 Blackburn Road, Clayton, VIC 3168, Australia

ABSTRACT Nanoparticle (NP) internalization by cells is complex, highly heterogeneous and fundamentally important for nanomedicine. We report powerful probabilistic statistics from single cell data on quantitative NP uptake for PEG coated- and transferrin receptor targeted-gold NPs for cancer-derived and fibroblast cells according to cell size, receptor expression and receptor density. The smaller cancer cells had a greater receptor density and more efficient uptake of targeted NPs. However, simply due to fibroblasts being larger with more receptors, they exhibit greater NP uptake. While highly heterogeneous, targeted NP uptake strongly correlated with receptor expression. When uptake was normalized to cell size, no correlation existed. Consequently, skewed population distributions in cell sizes explains the distribution in NP uptake. Furthermore, exposure to the transferrin receptor-targeted NPs alter fibroblast size and receptor expression suggesting that receptor targeted NPs may interfere with metabolic flux and nutrient exchange which could assist in explaining altered regulation of cells exposed to nanoparticles.

KEYWORDS

Nanoparticles, transferrin receptor, single cell analysis, cell size, receptor mediated endocytosis.

INTRODUCTION

Heterogenous uptake of therapeutics between cells leads to differential response, and compromises treatment outcomes [1]. Metal nanoparticle (NP) use for targeted biomedical applications are actively being developed; with many NP platforms reaching clinical trials and even approved for clinical use in diagnostics, cancer therapy, and drug delivery [2]. Despite the potential impact of metal NPs in therapeutics, heterogenous NP uptake between individual cells and different cell lines is not well characterized. Furthermore, NPs can also serve as excellent proxies for other targeted therapeutic formulations [3]. A deeper understanding of factors influencing NP association and uptake by single cells can facilitate improvements in delivery and therapeutic efficacy.

NP internalization into cells is predominately mediated via caveolin and/or receptor (or clathrin) dependent endocytosis [4-7] and further mediated by NP physicochemical properties such as size, shape, surface functionalization and charge [8, 9]. The surface of NPs are often modified to increase biocompatibility and enhance therapeutic effectiveness [10], but also in many applications, NPs are surface functionalized with ligands to bind with cell membrane receptors upregulated in the targeted cell population [6].

Transferrin receptor 1 (TfR1 or Cluster of Differentiation, CD71) is a protein responsible for iron uptake and transport within the cell [11-14]. Transferrin receptor 2 (TfR2) is a homologous but less understood companion to CD71 [15-17], specifically responsible for intracellular iron transport to the mitochondria [18] and iron homeostasis [19]. TfR2 expression has been measured in different cancer cell lines, with inter-cell line expression found to be inversely proportional to

that of CD71 [15, 20]. The overexpression of CD71 and TfR2 is typically found in many cancer cell lines compared to healthy [21] and benign cells [22], attributed to increased iron requirements [12]. Due to this overexpression, CD71 has served as an effective target for functionalized NPs [12, 23, 24].

Vesicle formation for internalization of extracellular material determines uptake [25] and nutritional flux in general [26]. Determinants of cell size, causes and effects, are tightly regulated and while topics of intensive research and postulation, mechanistic understanding remains elusive [27]. Increasing metabolic activity and nutritional requirements leads to an increase in cell surface area to accommodate upregulated receptors, endocytosis and nutritional flux into the cell to enable biochemical homeostasis since intracellular processes are strongly dependent on maintenance of biomolecular concentrations [26, 28].

Cells are innately heterogenous, and present greatly varying sizes and expression of receptors within a cell population. In bulk analysis, natural characteristic heterogeneity across a population can be disproportionally skewed by sub-populations, affecting measurements and potentially leading to incorrect conclusions [29]. For example, two cell populations can have statistically equivalent mean NP uptake, but the NP uptake distribution across the populations, spanning more than two orders of magnitude, can be statistically different [30].

Despite the immense interest in targeting NPs towards cancer cells, there is disproportionally little information available on factors that direct NP uptake at the individual cell level yet can drive macroscale or organism-level outcomes. This insight can only be reasonably achieved through single cell analysis, which has potential to reveal critical cell and NP attributes that can enhance efficacy of targeted delivery.

Retention of targeted NPs within the tumor microenvironment *in vivo* is being increasingly studied and recent studies challenge the paradigm that targeted NPs' fate are specifically in the cancer cell sub-population of a tumor [31]. Simultaneously, strategies that target stromal and immune cells including tumor associated fibroblasts are also rapidly accelerating [32-34]. Heterogeneity in cell populations is increasingly recognized and accurate population descriptions are required for modelling, conceptual understanding and identifying differential delivery of pharmaceuticals and response.

In this study, we quantitatively compared single cell population data from a prostate cancer (PC-3) cell line with upregulated CD71 [35] and a human fibroblast (HFF) cell line for association of transferrin functionalized gold (AuT) NPs. Association was compared to polyethylene glycol (PEG) coated gold NPs that are internalized via non-specific pathways. Quantitative synchrotron X-ray fluorescence microscopy images of gold NPs associated with individual cells were cross correlated with identical confocal images of both CD71 and TfR2. We present the first quantitative single cell analysis of NP association, without the use of labels, in individual cells as a function of cell surface area, total CD71 and TfR2 expression and the respective relative receptor densities. While targeting NPs to cancer cells is well regarded to increase uptake, here we provide quantitative analysis of targeted NP association correlated with the actual receptor expression at a single cell level. In this case we statistically describe the uptake as a function of receptor expression for individual cells across a cell population. The single cell data offers unique understanding of the cell population heterogeneity and probabilistic mathematical descriptions that can advance conceptual understanding of NP fate and cellular impact.

EXPERIMENTAL

Cell Culture. The prostate cancer cell line, PC-3 (ECACC, 90112714, passage #13) and a human fibroblast cell line, HFF (ATCC passage #8) were used. Both cell lines were cultured in RMPI media with 0.3g/L L-Glutamine (Life Technologies), supplemented with 5% Penicillin-Streptomycin (Life Technologies) and 10% fetal bovine serum (Life Technologies) and kept in a humidified incubator at 37°C and 5% CO2.

For confocal analysis, approximately 150,000 cells per well were plated in a flexiPERM 8-well slide (Sarstedt). After overnight cell adhesion, cells were incubated with ~2-3 nM NPs for 2 hours in a humidified incubator at 37°C.

NP Preparation. Gold seed solution was synthesized using the Turkevich method [36] to produce NPs with a diameter of 18 ± 2 nm as determined by DLS and 14.5 $\pm$ 2 nm (n=40) as determined by TEM. Gold-PEG (AuPEG) NPs were synthesized by adding a 400 µL mixture of short PEG (458.6g/mol, Polypure) and long PEG (5000g/mol, Rapp Polymere) at a molar ratio of 2:1 for 12 hours at 4°C to produce NPs with a diameter of 35 ± 2 nm. To develop Gold-Transferrin (AuT) NPs, the synthesized AuPEG NPs were crosslinked with a 150 µL mixture of 0.4 M 1-ethyl-3-(3-dimethylaminopropyl) carbodiimide (EDC) (Sigma-Aldrich) and 0.1 M N-hydroxysuccinimide (NHS) (Sigma-Aldrich) for 5 minutes at room temperature. 20 µL 500 µg/mL holo-human transferrin was then added to produce AuT NPs with a diameter of 38 ± 2 nm. After each step of synthesis, centrifugation of the NP solution at 14,000 G for 10 minutes was used to remove excess solution using a Hettich Zentrifugen Mikro 22 R centrifuge. NPs were characterized using transmission electron microscopy (JEOL JEM-2100F-HR Transmission Electron Microscope), dynamic light scattering (Malvern Instruments Zetasizer Nano ZS) and absorbance peaks were measured with the UV-Vis Spectroscopy (Thermo Evolution 201 UV-Vis

Spectrophotometer) to confirm successful synthesis (NP characterization presented in Figure S1 and Table S1).

Immunofluorescence staining. For confocal microscopy, cells were washed in PBS and fixed with 95% ethanol and 5% acetic acid on ice for 10 minutes. Cells were washed again with PBS, permeabilized in PBS containing 0.5% Triton X-100 for 15 minutes at 37°C. After permeabilisation, cells were subsequently washed and incubated at 37°C in PBS containing 5% goat serum for 1 hour to block non-specific binding. Anti-Transferrin Receptor 2/TfR2 antibody (Abcam) was used at a 1/200 dilution in PBS containing 1% goat serum and incubated for 1 hour at 37°C. After washing cells with PBS, cells incubated with Goat Anti-Mouse IgG Alexa Fluor 647 secondary antibody at a 1/500 dilution in 1% goat serum was added for 1 hour at 37°C. FITC Mouse Anti-Human CD71 (BD Biosciences) was used as described in the product sheet. Any dilutions were made in PBS containing 1% goat serum was incubated for 1 hour at 37°C. Lastly, 4',6-diamidino-2-phenylindole (DAPI) was added to the fixed cells at a 1/10000 dilution for 10 minutes at room temperature to allow identification of cell nuclei during imaging. Cells were rinsed thoroughly with Milli-Q water prior to confocal microscopy being performed.

Confocal Microscopy. A Zeiss LSM 710 laser scanning confocal microscope (Carl Zeiss) was used to acquire fluorescent image sets. Images were acquired with a 20x objective with a 405 nm laser for the DAPI channel, 488 nm laser for the CD71 channel and a 560 nm laser utilized for the TfR2 channel. Image dimensions were 7168 × 1024 pixels, corresponding to image size of 2.9 × 0.42 mm giving x and y resolutions of 0.415 μm. Z-stacks were utilized for each condition using 2 μm slice width and varied in depth between 24 μm to 72 μm based on sample requirements. Negative staining of CD71, TfR2 and DAPI fluorescent markers was performed and is displayed in Figure S2.

X-Ray Fluorescence (XRF). After confocal acquisition, the wells were washed with Milli-Q water and $CuSO_4$ at a concentration of 6.27 μM was added to the wells for 1 hour. After washing with Milli-Q water, wells were dried in preparation for X-ray fluorescence microscopy (XFM) analysis. XFM elemental analysis was conducted at the Australian Synchrotron X-ray fluorescence microscopy beamline [37]. To acquire high resolution images, a pixel size of 2 μm × 2 μm was used, with a pixel dwell of 4 μs. Quantification of elemental concentrations was based on scans of known composition and concentration reference thin foils (Micromatter). Gold elemental distribution maps were generated using GeoPIXE [38]. The elemental map images were saved in a tiff format, displaying pixel intensity values in ng/cm^2. A limit of quantification (0.5 pg) was taken as approximately three times the minimum detection limit for the largest cells.

Image and Data Analysis. 8-bit greyscale raw confocal images were exported from Zen Black software (Carl Zeiss). The copper elemental map was used as a mask to identify matching cells on the subsequent confocal images. By this process, the XRF gold elemental map was correlated with these confocal images and thereby, provided correlated image sets. These overlays were performed in Adobe Photoshop CC (2020 Adobe Systems Incorporated). The aligned image sets were exported as TIF files to MATLAB (MathWorks R2018a) for cell size and gold internalisation analysis. The DAPI maximum projection was used to define each individual cell nucleus and CD71 was used to mask the plasma membrane, i.e., the corresponding individual whole cell region. These masks were manually defined in MATLAB (Figure S3) using a combination of custom code and in-built image processing features.

RESULTS AND DISCUSSION

NP association as a function of cell size. Across the cell populations, heterogeneity in cell size, receptor expression and nanoparticle association was described by lognormal Probability Density Functions (PDFs);

$$\text{PDF} = \frac{1}{x\sigma\sqrt{2\pi}} \exp\left(-\frac{(\ln(x)-\mu)^2}{2\sigma^2}\right) \qquad (1)$$

where μ and σ are the lognormal distribution parameters which have dependence on variables' mean and variance. Median cell areas (in terms of the area exposed to media) for both the prostate cancer cell line, PC-3, and human fibroblast cell line, HFF, determined from confocal microscopy were 367 and 1025 μm^2 respectively (Figure S4A). Data are presented with their associated lognormal PDFs in Figure S4B along with the associated fitting parameters in Table S2. Not only are the HFF cells much larger (Wilcoxon rank sum test: $P < 0.0001$), but also demonstrate a higher degree of heterogeneity in cell area as demonstrated by the broader probability density function.

Identical cells imaged with confocal microscopy were then imaged by synchrotron X-ray fluorescence microscopy (XRM) for quantitative analysis of the gold NP association with each cell (Figure 1 and Table 1). This single cell correlative method is expanded on within the experimental section and the corresponding images are found in Figure S2. Associated PDFs and lognormal fitting parameters are displayed in Figure S5 and Table S3. AuT NPs are expected to be specifically taken up by cells via receptor-mediated endocytosis through transferrin receptor 1 (CD71) and transferrin receptor 2 (TfR2), although can also be internalized through non-specific pathways such as caveolin mediated endocytosis [39]. AuT NPs had much greater association with both the cancer and fibroblast cells compared to the AuPEG NPs, consistent with previous reports for cancer cell lines [40, 41]. HFF cells surprisingly, while having a lower mean association, had a greater median association of the targeted AuT NPs compared to PC-3 (Wilcoxon rank sum test

$P < 0.0001$), i.e., the 'normal'-tissue cells had greater median association of targeted NPs than did the overexpressing cancer cells. Furthermore, the AuT NP association was significantly and strongly correlated with cell size (Figure 2B and 2D). As cell area increases, association of the AuT NPs also increases, especially for the HFF cells. Conversely, no significant correlation between AuPEG NP association and cell size was observed (Figure 2A and 2C), although a weak positive correlation observed for the HFF cells was close to having significance. Wang et al. observed fluorescently labeled PEG coated Au NPs positively correlated with human mesenchymal stem cell size, but only 3 cells per condition were analyzed and the cell sizes were mechanically constricted to investigate physical properties of cells [42]. A very weak positive linear correlation in association of unfunctionalized fluorescent polystyrene NPs with MDA-MB-231 cell size was reported by Khetan et al [43]. While the significance of the correlation was not clear, the fitting provided insights that enabled powerful predictive modelling of NP association. An important distinction in the current work for the unfunctionalized NPs is that cells here were imaged in-situ, rather than being detached after exposure to NPs. With respect to the AuPEG NPs, although the PC-3 cells are substantially smaller than the HFF cells, NP association was comparable (Wilcoxon rank sum test $P = 0.47$). The endocytic process that AuPEG NPs undergo is by non-specific internalization, primarily through caveolin mediated endocytosis [44, 45]. Caveolin CAV-1 which modulates cell metabolism, has now been shown to be upregulated in several cancers and is linked to tumorigenesis [46, 47]. In this regard it is then unsurprising that the smaller cancer cells could take up more NPs relative to their size compared to the fibroblast cells. The unexpected result from this analysis though is that the fibroblast cells had greater numbers of the targeted AuT NPs associated than did the PC-3 cells. In this regard, NP association with respect to receptor expression was investigated.

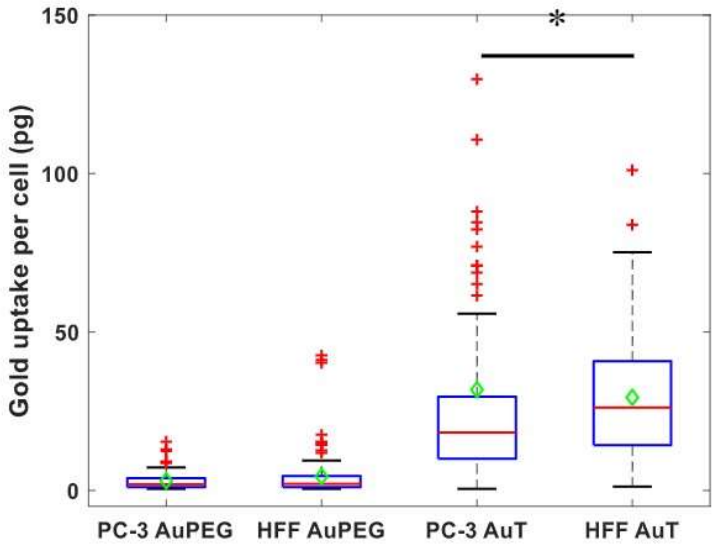

Figure 1. Association of NPs with cells increases ~7-fold with targeting functionality for both the cancer and fibroblast cells. Gold content per cell for AuPEG and AuT in PC-3 and HFF cell lines. Boxes contain 25-75 percentiles of the data, separated by the red horizontal line representing the median. Whiskers represent the 0.7 and 99.3 percentiles; red 'plus signs' indicate outliers; green diamonds represent the mean. * two-sided Wilcoxon rank sum test $P < 0.0001$.

Table 1. NP internalization statistics for the AuPEG and AuT NPs in PC-3 and HFF cell lines; including the mean, standard deviation, standard error in the mean, range, and the cell count. N.D.: not detected.

		n	Mean Au mass (pg)	Median (pg)	Interquartile range (pg)	Range (pg)
PC-3	AuPEG	73	3.03	1.96	1.04 - 3.83	N.D.-15.4
	AuT	221	31.8	18.3	10.0 – 29.6	N.D.-129.8
HFF	AuPEG	117	4.41	2.07	1.01 – 4.59	N.D.-42.6
	AuT	119	29.3	26.2	14.3 – 40.8	1.22-101.1

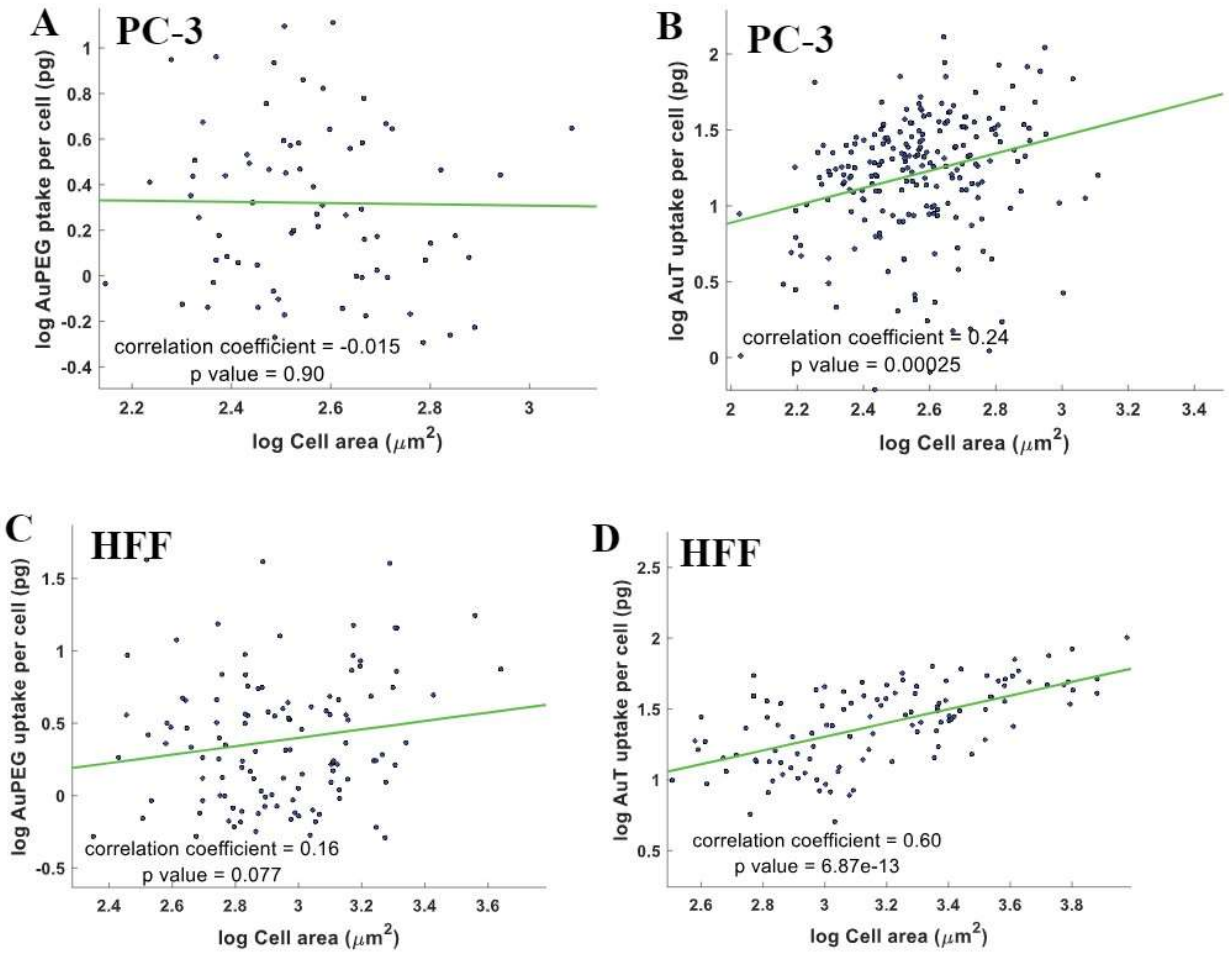

Figure 2. AuT NP association is correlated with an increasing cell area. Log-transformed scatterplots of cell area compared to the AuPEG (A) and AuT (B) NP uptake in the PC-3 cell line and the AuPEG (C) and AuT (D) NP association in the HFF cell line.

Relationship between TfR expression and NP association. AuT NPs should primarily be internalized by actively binding CD71 and TfR2 [48] and thus, the transferrin receptors were stained in both cell lines. Figure S2 demonstrates negative staining of CD71 and TfR2. As we observed that HFF cells have a greater association with AuT NPs compared to the PC-3 cells, it

could be explained by the HFF exhibiting a higher expression in absolute terms of either, or both transferrin receptors. Indeed, Figures 3A and 3C show that HFF cell populations cocultured with either AuPEG or AuT NPs exhibit greater CD71 expression compared to PC-3 cells. Considering receptor density however, the PC-3 cells exhibit a much greater expression of CD71 receptors per cell area compared to the HFF cells (Figures 3B and 3D). A summary of the mean, median and lognormal fitting parameters for each condition is given in Table 2. A curious discovery was that the AuT NPs alter transferrin receptor expression, specifically for the HFF cells where the distribution skews towards an increase in the number of cells expressing greater numbers of receptors after AuT NPs exposure (two-sided Wilcoxon rank sum test: $P < 0.0001$). This upregulation could be explained by AuT NPs impeding transport of nutritional requirements and homeostasis but is not observed for the cancer cell line. Another notable observation is that with upregulation of CD71 expression upon exposure to the AuT NPs the PDF transforms toward a normal distribution for receptor density (Figure 3B and 3D), indicating a proportionality between receptor expression and cell size. This is consistent with observations where, to maintain homeostasis, protein concentration is conserved across variable cell sizes [49]; a phenomenon supported here in that CD71 expression significantly increases, yet receptor density is preserved (two-sided Wilcoxon rank sum test $P = 0.18$).

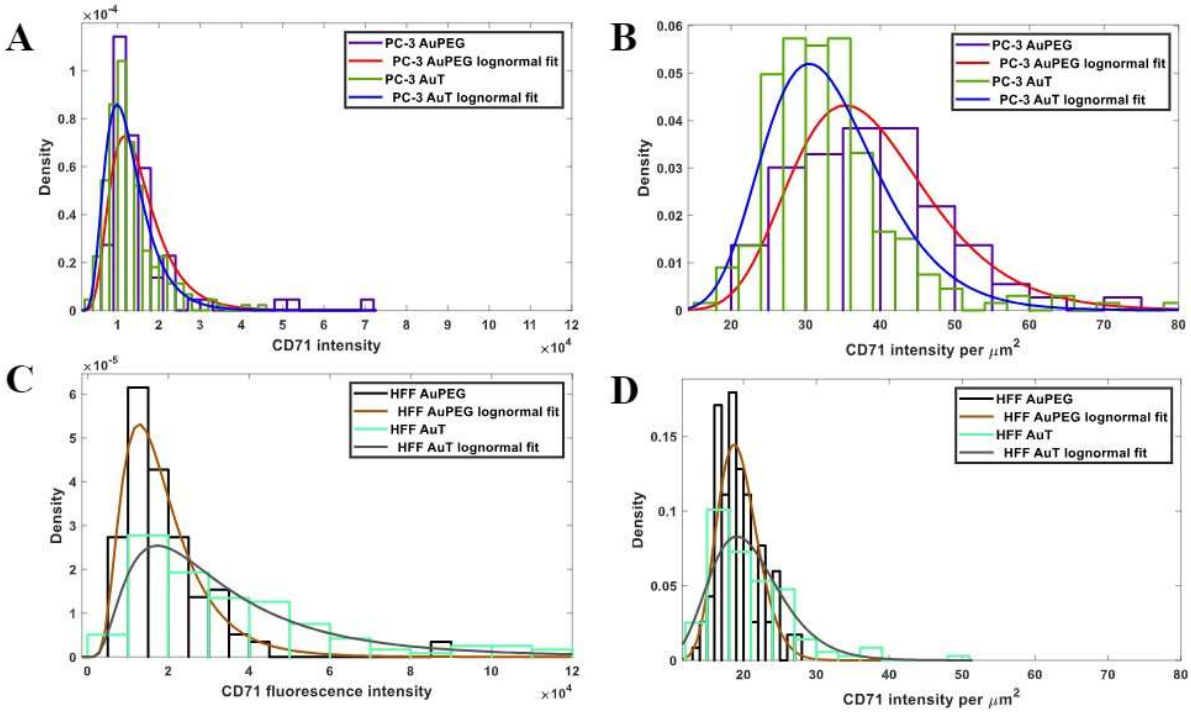

Figure 3. HFF cells have greater CD71 expression while PC-3 cells have greater receptor expression density. Probability density functions of the CD71 fluorescence intensity (indicative of TfR1 expression) of the PC-3 (A) and HFF (C) cell lines and CD71 density measured by CD71 fluorescence intensity per cell area in μm^2 for the PC-3 (B) and HFF (D) cell lines.

Table 2. Evaluated statistics of the CD71 fluorescence intensity and CD71 density (CD71 fluorescence intensity per cell area in μm^2) and lognormal fitting parameters for the PC-3 and HFF cell lines.

	NP	n	Condition	Mean	Median	μ	σ
PC-3	AuPEG	73	CD71 intensity	15690	12639	9.55	0.430
			CD71 intensity per cell area	38.89	38.66	3.63	0.253
	AuT	221	CD71 intensity	13036	11535	9.38	0.430
			CD71 intensity per cell area	33.41	31.96	3.48	0.244
HFF	AuPEG	117	CD71 intensity	19173	16260	9.72	0.515
			CD71 intensity per cell area	19.31	18.73	2.95	0.146
	AuT	119	CD71 intensity	36367	27302	10.3	0.708
			CD71 intensity per cell area	20.92	19.15	3.01	0.244

When comparing the single cell analysis of the CD71 fluorescence intensity between the PC-3 and HFF cell lines, a higher expression of CD71 was found in the HFF cell line. Median values indicate expression in the HFF cells was more than 2-times greater compared to PC-3 cells for the AuT NP exposure. A greater absolute expression of CD71 in the HFF cells is linked to a greater AuT NP association than for the PC-3 cell line. However, the PC-3 cells have an approximately two to three times greater receptor density compared to the HFF cells and NP association is consequently more comparable. No correlation between NP association and receptor density (i.e., receptor number was normalized by cell size) on individual cells was observed (Figure S6). Therefore, cell area is an important variable directly mediating the internalization of actively targeted NPs.

Transferrin receptor 2 (TfR2) is a homologous companion to CD71 also involved in recruitment of transferrin [48]. As internalization of AuT NPs could be dependent on either transferrin receptors, NP association relative to TfR2 association was also evaluated. TfR2 fluorescence intensity and TfR2 density per cell area in μm^2 were analyzed by single cell analysis for both the PC-3 and HFF cell lines with both NP conditions (Figure S7 and Table 3).

Table 3. Evaluated statistics of the TfR2 fluorescence intensity and TfR2 density (TfR2 fluorescence intensity per cell area in μm^2) and lognormal fitting parameters for the PC-3 and HFF cell lines.

	NP	n	Condition	Mean	Median	μ	σ
PC-3	AuPEG	73	TfR2 intensity	5728	4848	8.54	0.459
			TfR2 intensity per cell area	14.16	14.22	2.62	0.256
	AuT	221	TfR2 intensity	6388	5855	8.67	0.437
			TfR2 intensity per cell area	16.62	16.03	2.76	0.303
HFF	AuPEG	117	TfR2 intensity	5647	4690	8.47	0.531
			TfR2 intensity per cell area	5.77	5.43	1.70	0.302
	AuT	119	TfR2 intensity	11224	9563	9.14	0.616
			TfR2 intensity per cell area	7.43	6.12	1.89	0.465

The expression and distribution of TfR2 had a similar trend to that of CD71 (Figure 3), in that the HFF cell line expresses more TfR2 than PC-3. The CD71 fluorescence was approximately 2-3 times higher in the PC-3 cell line and 3-4 times higher in the HFF cell line than the TfR2 fluorescence, however this cannot be considered quantitative. Expression of each receptor is highly correlated within each cell population (Figure S8). For the PC-3 cell line, the TfR2 expression

increased after AuT exposure (two-sided Wilcoxon rank sum test: $P = 0.021$), unlike the CD71 expression. This may suggest a domination or saturation of one receptor compared to the other for PC-3 cells. While the PC-3 cell receptor expression increases, cell size remained constant (two-sided Wilcoxon rank sum test: $P = 0.89$) resulting in an increased receptor density. For the HFF cells, TfR2 increases with AuT ($P < 0.0001$) with a corresponding increase in cell size such that receptor density is mostly conserved (Figure S7D).

NP association with each cell type was then compared with respect to receptor expression and receptor density for individual cells, presented as scatter plots in Figure 4. As the AuPEG NP is expected to be internalized by caveolin mediated processes, the association data has little to no correlation with CD71 and TfR2 fluorescence intensities in both the PC-3 and HFF cell lines. However, AuT NP associations are strongly correlated with receptor expression, indicating that internalization is mediated by CD71 and TfR2 receptors. We also observe that the PC-3 cells are more efficient in NP uptake than HFF cells when we compare NP association relative to receptor expression (Figure 5). Associated PDFs and lognormal fitting parameters are displayed in Figure S9 and Table S4. The PC-3 cell line was more efficient in AuT NP association when compared to the larger HFF cells with consideration of receptor density expression for both CD71 and TfR2; demonstrating the importance of the receptor density. There was no correlation between NP association and receptor density (Figure S5), confirming the dependence of NP uptake on cell size.

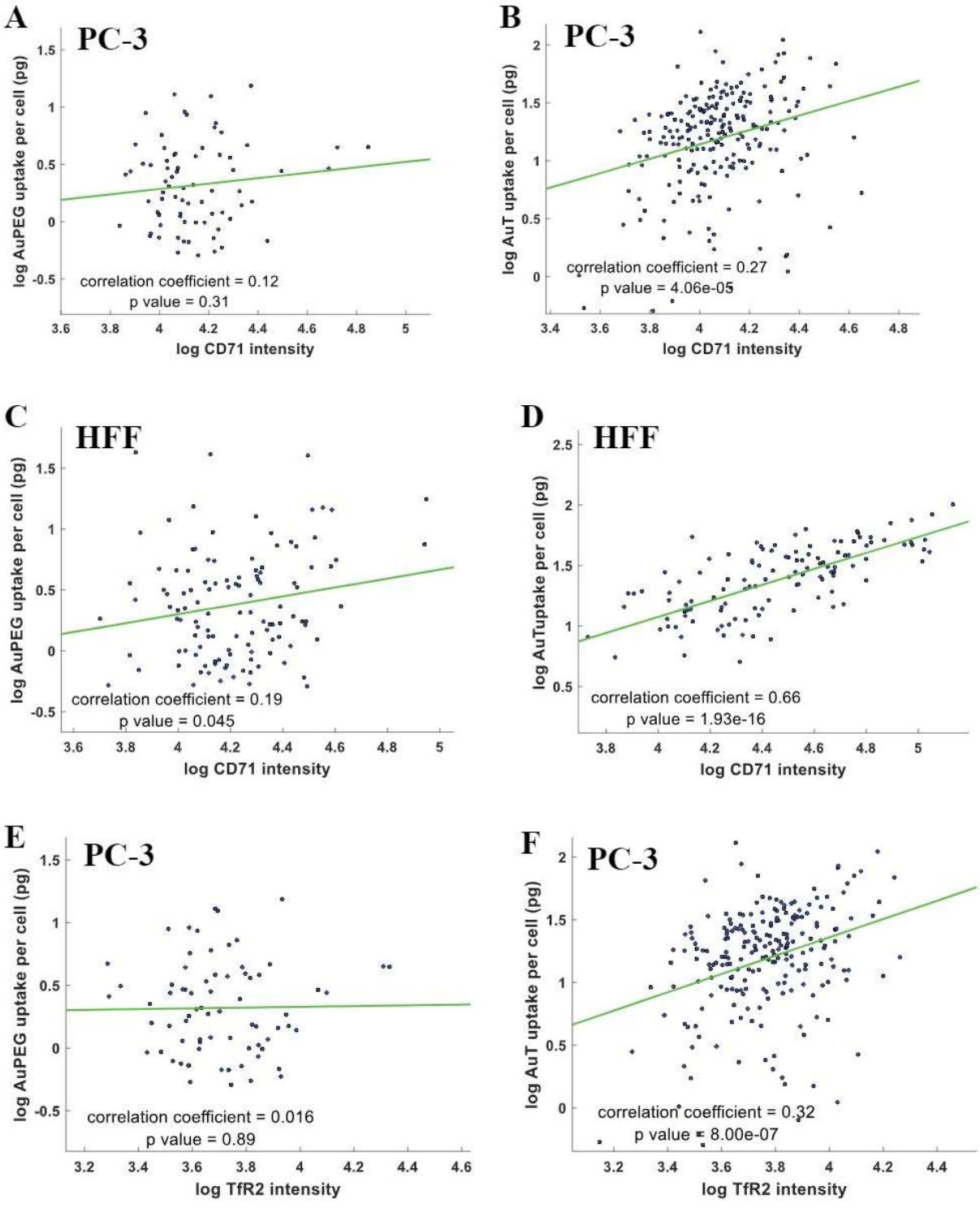
A
PC-3
log AuPEG uptake per cell (pg)
correlation coefficient = 0.12
p value = 0.31
log CD71 intensity
B
PC-3
log AuT uptake per cell (pg)
correlation coefficient = 0.27
p value = 4.06e-05
log CD71 intensity
C
HFF
log AuPEG uptake per cell (pg)
correlation coefficient = 0.19
p value = 0.045
log CD71 intensity
D
HFF
log AuTuptake per cell (pg)
correlation coefficient = 0.66
p value = 1.93e-16
log CD71 intensity
E
PC-3
log AuPEG uptake per cell (pg)
correlation coefficient = 0.016
p value = 0.89
log TfR2 intensity
F
PC-3
log AuT uptake per cell (pg)
correlation coefficient = 0.32
p value = 8.00e-07
log TfR2 intensity

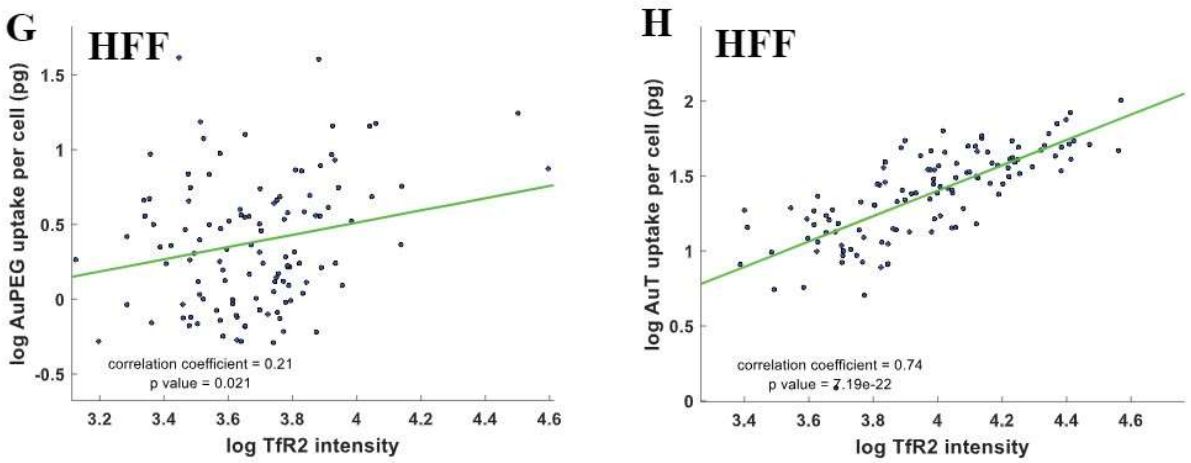

Figure 4. Targeted NP association is correlated with receptor expression. Log-transformed scatterplots of CD71 (TfR1) fluorescence intensity compared to the AuPEG (A) and AuT (B) NP association in the PC-3 cell line and the AuPEG (C) and AuT (D) NP association in the HFF cell line. The TfR2 fluorescence intensity for the AuPEG (E) and AuT (F) NP association in the PC-3 cell line and the AuPEG (G) and AuT (H) NP association in the HFF cell line.

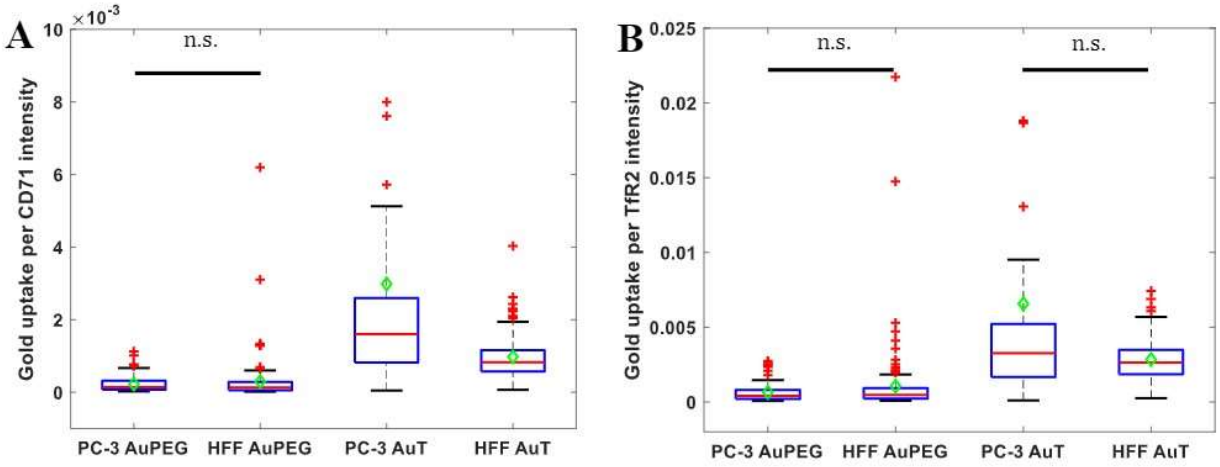

Figure 5. Relative to receptor expression, PC-3 cells more efficiently internalize NPs. Gold association per cell for AuPEG and AuT per receptor intensity for CD71 (A) and TfR2 (B) in PC-

3 and HFF cell lines. The box and whisker properties are the same as in Figure 1. n.s.: indicates non-significant but otherwise all comparisons are significant: $P < 0.0005$; Kruskal-Wallis test with Bonferroni correction and pairwise comparison.

The data suggests that targeted AuT NPs may interfere with nutrient exchange and metabolic flux which in-turn instigates a change in cell size to accommodate upregulation of receptor expression. Under this interpretation, enlargement of the cells and increasing expression of transferrin receptors maintains the cells' biosynthesis capacity. In other models of nanoparticle uptake heterogeneity [25], it has been assumed that within time constraints cell size is static, and alternatively may shrink in response to NP toxicity. Contrary to this, our data shows that in short time frames, cell size can increase in response to NP exposure. We propose this is due to targeted nanoparticles interfering with nutritional transport, instigating an upregulation of processes to increase cell surface area to maintain nutritional demands and homeostasis. This would be one contributing effect to explain how gold nanoparticles, often considered to be biologically inert, perturb gene expression [50, 51]. In this interpretation it is important to clarify that we consider receptor expression to be dependent on cell size, i.e. the larger cell size facilitates the capacity to express more receptors, opposed to the converse consideration that the number of expressed receptors defines the cell size. Consequently, we consider that the cell will define its cell size to enable expression of the receptor numbers desired to be able to maintain a nutritional influx to maintain intracellular biochemical concentrations and reactions. This interpretation is supported by the data indicating that a constant receptor density is maintained.

Both HFF cells and cancerous PC-3 cells preferentially associated transferrin receptor targeted NPs over PEG-coated NPs. While the PC-3 cells have significantly greater receptor density than HFF cells and more efficient association of NPs in terms of NP association per receptor, the HFF cells still had a greater NP association than the PC-3, attributed simply to the much larger size of the HFF cells and consequently a greater absolute number of receptors. There is a subtle, but important distinction that NP association is dependent on cell size rather than just considering the total number of receptors in that the receptor density is highly variable between cell types. As histopathological examination of biopsies principally identifies cells based on marker density, the greater uptake of targeted NP-based therapeutics may have impactful implications in that cells appearing as 'negative' could have comparable NP uptake. This raises questions about the ability to deliver targeted nanoparticles to specific cell populations, especially if they're physically small. The data here highlights that it is important to recognize that normal cells express the same receptors identified as being upregulated and characteristic of cancer cells. It is inevitable that targeted nanoparticles will also be internalized by healthy cells in vivo. The extent of uptake by normal cells will be dependent on their nutritional requirements and the number of receptors, and invariably dependent on the cell size. The data here warrant in vivo investigation into how cell size could be an important factor in targeted nanoparticle fate, where either opportunities for improving therapeutic delivery, or identification of origins of off-target toxicities could present.

CONCLUSION

Nutritional requirements to maintain intracellular biochemistry mediate cell size to express receptors responsible for nutritional and metabolic flux. The data here also suggests that targeted

nanoparticles can interfere with nutrient flux which may be an explanation as to how nanoparticles alter cell expression.

AUTHOR INFORMATION

Corresponding Author

Ivan Kempson – University of South Australia, Mawson Lakes, S.A., 5095, Australia. https://orcid.org/0000-0002-3886-9516 Email: Ivan.Kempson@unisa.edu.au

Author Contributions

The manuscript was written through contributions of all authors. All authors have given approval to the final version of the manuscript.

SUPPORTING INFORMATION

Characterization of NPs, including TEM, UV-Vis Spectroscopy and DLS measurements; Supporting Information of confocal microscopy fluorescent marker negative staining; cell size; probability density functions of gold NP uptake; scatterplots of NP uptake when compared to receptor density; scatterplots of CD71 and TfR2 receptor relationship; probability density functions of NP uptake per receptor intensity.

The following files are available free of charge.

Supporting Information (PDF)

ACKNOWLEDGMENT

This research was supported by the Australian Government through the Australian Research Council's Discovery Projects funding scheme (project no. DP190102119); the X-ray Fluorescence Microscopy beamline at the Australian

Synchrotron, part of ANSTO; and the facilities, scientific and technical assistance of Microscopy Australia, funded by the University of South Australia, State and Federal Governments.

REFERENCES

1. Qian, M., D.C. Wang, H. Chen, and Y. Cheng, *Detection of single cell heterogeneity in cancer.* Seminars in Cell & Developmental Biology, 2017. **64**: p. 143-149.
2. Anselmo, A.C. and S. Mitragotri, *Nanoparticles in the clinic: An update.* Bioengineering & translational medicine, 2019. **4**(3): p. e10143-e10143.
3. Zhang, Y., H. Yang, D. Wei, X. Zhang, J. Wang, X. Wu, and J. Chang, *Mitochondria-targeted nanoparticles in treatment of neurodegenerative diseases.* Exploration, 2021. **1**(3): p. 20210115.
4. Behzadi, S., V. Serpooshan, W. Tao, M.A. Hamaly, M.Y. Alkawareek, E.C. Dreaden, D. Brown, A.M. Alkilany, O.C. Farokhzad, and M. Mahmoudi, *Cellular uptake of nanoparticles: journey inside the cell.* Chemical Society reviews, 2017. **46**(14): p. 4218-4244.
5. Zhu, J., L. Liao, L. Zhu, P. Zhang, K. Guo, J. Kong, C. Ji, and B. Liu, *Size-dependent cellular uptake efficiency, mechanism, and cytotoxicity of silica nanoparticles toward HeLa cells.* Talanta, 2013. **107**: p. 408-415.
6. Yameen, B., W.I. Choi, C. Vilos, A. Swami, J. Shi, and O.C. Farokhzad, *Insight into nanoparticle cellular uptake and intracellular targeting.* Journal of Controlled Release, 2014. **190**: p. 485-499.
7. dos Santos, T., J. Varela, I. Lynch, A. Salvati, and K.A. Dawson, *Quantitative Assessment of the Comparative Nanoparticle-Uptake Efficiency of a Range of Cell Lines.* Small, 2011. **7**(23): p. 3341-3349.
8. Zhang, S., H. Gao, and G. Bao, *Physical Principles of Nanoparticle Cellular Endocytosis.* ACS Nano, 2015. **9**(9): p. 8655-8671.
9. Vácha, R., F.J. Martinez-Veracoechea, and D. Frenkel, *Receptor-Mediated Endocytosis of Nanoparticles of Various Shapes.* Nano Letters, 2011. **11**(12): p. 5391-5395.
10. Tang, G., J. He, J. Liu, X. Yan, and K. Fan, *Nanozyme for tumor therapy: Surface modification matters.* Exploration, 2021. **1**(1): p. 75-89.
11. Aisen, P., *Transferrin receptor 1.* The International Journal of Biochemistry & Cell Biology, 2004. **36**(11): p. 2137-2143.
12. Shen, Y., X. Li, D. Dong, B. Zhang, Y. Xue, and P. Shang, *Transferrin receptor 1 in cancer: a new sight for cancer therapy.* American journal of cancer research, 2018. **8**(6): p. 916-931.
13. Lok, C.N. and T.T. Loh, *Regulation of transferrin function and expression: review and update.* Biol Signals Recept, 1998. **7**(3): p. 157-78.
14. Ponka, P. and C.N. Lok, *The transferrin receptor: role in health and disease.* The International Journal of Biochemistry & Cell Biology, 1999. **31**(10): p. 1111-1137.

15. Calzolari, A., I. Oliviero, S. Deaglio, G. Mariani, M. Biffoni, N.M. Sposi, F. Malavasi, C. Peschle, and U. Testa, *Transferrin receptor 2 is frequently expressed in human cancer cell lines.* Blood Cells, Molecules, and Diseases, 2007. **39**(1): p. 82-91.
16. Chen, J., J. Wang, K.R. Meyers, and C.A. Enns, *Transferrin-directed internalization and cycling of transferrin receptor 2.* Traffic (Copenhagen, Denmark), 2009. **10**(10): p. 1488-1501.
17. Trinder, D. and E. Baker, *Transferrin receptor 2: a new molecule in iron metabolism.* The International Journal of Biochemistry & Cell Biology, 2003. **35**(3): p. 292-296.
18. Khalil, S., M. Holy, S. Grado, R. Fleming, R. Kurita, Y. Nakamura, and A. Goldfarb, *A specialized pathway for erythroid iron delivery through lysosomal trafficking of transferrin receptor 2.* Blood Advances, 2017. **1**(15): p. 1181-1194.
19. Roetto, A., M. Mezzanotte, and R.M. Pellegrino, *The Functional Versatility of Transferrin Receptor 2 and Its Therapeutic Value.* Pharmaceuticals, 2018. **11**(4): p. 115.
20. Adachi, M., K. Kai, K. Yamaji, T. Ide, H. Noshiro, A. Kawaguchi, and S. Aishima, *Transferrin receptor 1 overexpression is associated with tumour de-differentiation and acts as a potential prognostic indicator of hepatocellular carcinoma.* Histopathology, 2019. **75**(1): p. 63-73.
21. Singh, M., K. Mugler, D.W. Hailoo, S. Burke, B. Nemesure, K. Torkko, and K.R. Shroyer, *Differential Expression of Transferrin Receptor (TfR) in a Spectrum of Normal to Malignant Breast Tissues: Implications for In Situ and Invasive Carcinoma.* Applied Immunohistochemistry & Molecular Morphology, 2011. **19**(5): p. 417-423.
22. Högemann-Savellano, D., E. Bos, C. Blondet, F. Sato, T. Abe, L. Josephson, R. Weissleder, J. Gaudet, D. Sgroi, P.J. Peters, and J.P. Basilion, *The Transferrin Receptor: A Potential Molecular Imaging Marker for Human Cancer.* Neoplasia, 2003. **5**(6): p. 495-506.
23. Chan, K.T., M.Y. Choi, K.K.Y. Lai, W. Tan, L.N. Tung, H.Y. Lam, D.K.H. Tong, N.P. Lee, and S. Law, *Overexpression of transferrin receptor CD71 and its tumorigenic properties in esophageal squamous cell carcinoma.* Oncol Rep, 2014. **31**(3): p. 1296-1304.
24. Li, H. and Z.M. Qian, *Transferrin/transferrin receptor-mediated drug delivery.* Med Res Rev, 2002. **22**(3): p. 225-50.
25. Rees, P., J.W. Wills, M.R. Brown, C.M. Barnes, and H.D. Summers, *The origin of heterogeneous nanoparticle uptake by cells.* Nature Communications, 2019. **10**(1): p. 2341.
26. Marshall, W.F., K.D. Young, M. Swaffer, E. Wood, P. Nurse, A. Kimura, J. Frankel, J. Wallingford, V. Walbot, X. Qu, and A.H.K. Roeder, *What determines cell size?* BMC Biology, 2012. **10**(1): p. 101.
27. Vargas-Garcia, C.A., K.R. Ghusinga, and A. Singh, *Cell size control and gene expression homeostasis in single-cells.* Current Opinion in Systems Biology, 2018. **8**: p. 109-116.
28. Padovan-Merhar, O., Gautham P. Nair, Andrew G. Biaesch, A. Mayer, S. Scarfone, Shawn W. Foley, Angela R. Wu, L.S. Churchman, A. Singh, and A. Raj, *Single Mammalian Cells Compensate for Differences in Cellular Volume and DNA Copy Number through Independent Global Transcriptional Mechanisms.* Molecular Cell, 2015. **58**(2): p. 339-352.

29. Kravchenko-Balasha, N., *Translating Cancer Molecular Variability into Personalized Information Using Bulk and Single Cell Approaches.* PROTEOMICS, 2020. **20**(13): p. 1900227.
30. Turnbull, T., B. Thierry, and I. Kempson, *A quantitative study of intercellular heterogeneity in gold nanoparticle uptake across multiple cell lines.* Analytical and bioanalytical chemistry., 2019. **411**(28): p. 7529-7538.
31. Korangath, P., D. Barnett James, A. Sharma, T. Henderson Elizabeth, J. Stewart, S.-H. Yu, K. Kandala Sri, C.-T. Yang, S. Caserto Julia, M. Hedayati, D. Armstrong Todd, E. Jaffee, C. Gruettner, C. Zhou Xian, W. Fu, C. Hu, S. Sukumar, W. Simons Brian, and R. Ivkov, *Nanoparticle interactions with immune cells dominate tumor retention and induce T cell–mediated tumor suppression in models of breast cancer.* Science Advances. **6**(13): p. eaay1601.
32. Valkenburg, K.C., A.E. de Groot, and K.J. Pienta, *Targeting the tumour stroma to improve cancer therapy.* Nature Reviews Clinical Oncology, 2018. **15**(6): p. 366-381.
33. Prakash, J., *Cancer-Associated Fibroblasts: Perspectives in Cancer Therapy.* Trends in Cancer, 2016. **2**(6): p. 277-279.
34. Kalluri, R. and M. Zeisberg, *Fibroblasts in cancer.* Nature Reviews Cancer, 2006. **6**(5): p. 392-401.
35. Deng, Z., D.H. Manz, S.V. Torti, and F.M. Torti, *Iron-responsive element-binding protein 2 plays an essential role in regulating prostate cancer cell growth.* Oncotarget, 2017. **8**(47): p. 82231-82243.
36. Turkevich, J., P.C. Stevenson, and J. Hillier, *A study of the nucleation and growth processes in the synthesis of colloidal gold.* Discussions of the Faraday Society, 1951. **11**(0): p. 55-75.
37. Howard, D.L., M.D. de Jonge, N. Afshar, C.G. Ryan, R. Kirkham, J. Reinhardt, C.M. Kewish, J. McKinlay, A. Walsh, J. Divitcos, N. Basten, L. Adamson, T. Fiala, L. Sammut, and D.J. Paterson, *The XFM beamline at the Australian Synchrotron.* Journal of Synchrotron Radiation, 2020. **27**(5): p. 1447-1458.
38. Ryan, C.G., *Quantitative trace element imaging using PIXE and the nuclear microprobe.* International Journal of Imaging Systems and Technology, 2000. **11**(4): p. 219-230.
39. Wang, Z., C. Tiruppathi, R.D. Minshall, and A.B. Malik, *Size and dynamics of caveolae studied using nanoparticles in living endothelial cells.* ACS nano, 2009. **3**(12): p. 4110-4116.
40. Nag, M., V. Gajbhiye, P. Kesharwani, and N.K. Jain, *Transferrin functionalized chitosan-PEG nanoparticles for targeted delivery of paclitaxel to cancer cells.* Colloids and Surfaces B: Biointerfaces, 2016. **148**: p. 363-370.
41. Jadia, R., J. Kydd, and P. Rai, *Remotely Phototriggered, Transferrin-Targeted Polymeric Nanoparticles for the Treatment of Breast Cancer.* Photochemistry and Photobiology, 2018. **94**(4): p. 765-774.
42. Wang, X., X. Hu, J. Li, A.C.M. Russe, N. Kawazoe, Y. Yang, and G. Chen, *Influence of cell size on cellular uptake of gold nanoparticles.* Biomaterials Science, 2016. **4**(6): p. 970-978.
43. Khetan, J., M. Shahinuzzaman, S. Barua, and D. Barua, *Quantitative Analysis of the Correlation between Cell Size and Cellular Uptake of Particles.* Biophysical Journal, 2019. **116**(2): p. 347-359.

44. Chen, J., L. Cao, Y. Cui, K. Tu, H. Wang, and L.-Q. Wang, *The exploration of endocytic mechanisms of PLA-PEG nanoparticles prepared by coaxialtri-capillary electrospray-template removal method.* Colloids and Surfaces B: Biointerfaces, 2018. **161**: p. 10-17.
45. Lühmann, T., M. Rimann, A.G. Bittermann, and H. Hall, *Cellular Uptake and Intracellular Pathways of PLL-g-PEG-DNA Nanoparticles.* Bioconjugate Chemistry, 2008. **19**(9): p. 1907-1916.
46. Qian, X.-L., Y.-H. Pan, Q.-Y. Huang, Y.-B. Shi, Q.-Y. Huang, Z.-Z. Hu, and L.-X. Xiong, *Caveolin-1: a multifaceted driver of breast cancer progression and its application in clinical treatment.* OncoTargets and therapy, 2019. **12**: p. 1539-1552.
47. Nwosu, Z.C., M.P. Ebert, S. Dooley, and C. Meyer, *Caveolin-1 in the regulation of cell metabolism: a cancer perspective.* Molecular Cancer, 2016. **15**(1): p. 71.
48. West, A.P., M.J. Bennett, V.M. Sellers, N.C. Andrews, C.A. Enns, and P.J. Bjorkman, *Comparison of the Interactions of Transferrin Receptor and Transferrin Receptor 2 with Transferrin and the Hereditary Hemochromatosis Protein HFE*.* Journal of Biological Chemistry, 2000. **275**(49): p. 38135-38138.
49. Mena, A., D.A. Medina, J. García-Martínez, V. Begley, A. Singh, S. Chávez, M.C. Muñoz-Centeno, and J.E. Pérez-Ortín, *Asymmetric cell division requires specific mechanisms for adjusting global transcription.* Nucleic Acids Research, 2017. **45**(21): p. 12401-12412.
50. Turnbull, T., M. Douglass, N.H. Williamson, D. Howard, R. Bhardwaj, M. Lawrence, D.J. Paterson, E. Bezak, B. Thierry, and I.M. Kempson, *Cross-Correlative Single-Cell Analysis Reveals Biological Mechanisms of Nanoparticle Radiosensitization.* ACS Nano, 2019. **13**(5): p. 5077-5090.
51. Falagan-Lotsch, P., E.M. Grzincic, and C.J. Murphy, *One low-dose exposure of gold nanoparticles induces long-term changes in human cells.* Proceedings of the National Academy of Sciences, 2016. **113**(47): p. 13318.

Graphical abstract: